Predictor-based Adaptive Incremental Nonlinear Dynamic Inversion for Fault-Tolerant Flight Control*

Chang, Jing; Guo, Zongyi; De Breuker, Roeland; Wang, Xuerui

DOI
10.1016/j.ifacol.2022.07.214

Publication date
2022

Document Version
Final published version

Published in
IFAC-PapersOnline

Available online at www.sciencedirect.com

ScienceDirect

IFAC PapersOnline CONFERENCE PAPER ARCHIVE

IFAC PapersOnLine 55-6 (2022) 730–736

Predictor-based Adaptive Incremental Nonlinear Dynamic Inversion for Fault-Tolerant Flight Control

Jing Chang * **Zongyi Guo** *** **Roeland De Breuker** ** **Xuerui Wang** **

* *School of Aerospace Science and Technology, Xidian University, Xi'an, 710126, China (e-mail: jchang@xidian.edu.cn).*

** *Delft University of Technology; Kluyverweg 1, 2629HS, Delft, The Netherlands. (e-mail: X.Wang-6@tudelft.nl, R.DeBreuker@tudelft.nl)*

*** *Northwestern Polytechnical University, Xi'an, 710072, China, (e-mail: guozongyi@nwpu.edu.cn)*

Abstract: The sensor-based Incremental Nonlinear Dynamic Inversion (INDI) control has shown promising robustness in the aerospace research field. This control framework only requires a partial knowledge of plant (control effectiveness) because of its usage of angular accelerations and actuator output measurements. However, there are still un-negligible uncertainties of the control effectiveness model in the flight control system, especially when the aircraft is subjected to structural damage/actuator faults. This paper shows that the conventional INDI control fails to satisfy the sufficient conditions for closed-loop stability in the presence of severe damage. Therefore, this paper also proposes a predictor-based gain adaptive INDI control (named PGA-INDI) which can successfully deal with control effectiveness parametric errors caused by structural damage, actuator faults, and model uncertainties. Various simulations using a public aircraft model have demonstrated the effectiveness of the proposed approach.

Keywords: Fault-tolerant Flight Control, Incremental Nonlinear Dynamic Inversion, Predictor, Control Effectiveness Uncertainty.

1. INTRODUCTION

There is no doubt that aerospace systems are becoming more intelligent, more autonomous, and more connected. Modern aerospace vehicles can be affected by extremely challenging uncertainties and new fault modes due to rising system complexity and critical fight conditions. It can be demonstrated that improving the performances of the Fault Detection and Diagnosis (FDD), Fault-Tolerant Control (FTC), and Fault-Tolerant Guidance (FTG) in the flight control system can not only enhance the safety of the system but also allows designers to optimize the aircraft structural design (weight saving) and thus to improve the aircraft performance and to decrease its environmental footprint (less fuel consumption and noise).

Many researchers have focused on the development of the methodologies for Fault-Tolerant Flight Control (FTFC) systems, among which model-based fault diagnosis and identification, Fault Estimation (FE), and active fault-tolerant control (pseudo-inverse technique, multiple models, adaptive control, observer-based control) have many advantages due to their high fault-tolerant ability. The development and current status of FDD and FTC and their application on aerospace are reviewed in Bošković and Mehra (2003); Zhang and Jiang (2008); Jiang and Yu (2012); Zolghadri et al. (2014). Among these works, the sensor-based incremental nonlinear control has shown its promising robustness in flight control (Sieberling et al. (2010); van Ekeren et al. (2018); Smeur et al. (2016)). The Incremental Nonlinear Dynamic Inversion (INDI) control scheme is to counteract (a part of) the nonlinear flight dynamics with the help of sensor measurements/estimates and derive a control law with incremental modulation for the resulting system. Compared to the conventional techniques, INDI methods make the controller has the fault-tolerant ability and reduced model-dependency, which are essential for safety-critical systems such as aircraft and aerospace vehicle. More recently, this technique has been applied in practice for quadrotors (Sun et al. (2020)), small unmanned aircraft (van Ekeren et al. (2018)) and a business jet aircraft (Keijzer et al. (2019)).

In the literature, only a few attempts have been made on stability and control performance analysis of the INDI control methods (Jeon et al. (2021); Wang et al. (2019b)). The sufficient conditions for the closed-loop stability of the INDI have been given in Wang et al. (2019b). Ensuring accurate estimations of angular acceleration and control effectiveness matrix is the key to enhancing the robustness of INDI. In practice, this can be violated in a harsh environment, unexpected faults, and unknown disturbances. Therefore, we need to develop an INDI control method with high adaptivity and can relax the estimation accuracy requirement on the control effectiveness matrix.

⋆ This work was supported by the National Natural Science Foundation of China under Grant 62003252, 62073254.

10.1016/j.ifacol.2022.07.214

In this paper, a novel predictor-based gain adaptive INDI control (denoted as PGA-INDI) is proposed. First, the conditions for the closed-loop stability of conventional INDI will be explored. Second, a predictor-based adaptive technique is proposed to enhance the robustness of the INDI method against uncertainties in the control effectiveness matrix. Third, simulations are performed to show the effectiveness of the proposed method in fault-tolerant flight control problems.

The rest of the paper is organized as follows: In section 2, the aircraft attitude dynamics modeling with actuator faults and structural damages are established. Section 3 introduces the predictor-based adaptive INDI control design. The simulation results are performed in Section 4. Section 5 concludes this paper.

2. AIRCRAFT DYNAMIC MODELING WITH ACTUATOR FAULTS AND STRUCTURAL DAMAGE

The normal six degrees of freedom nonlinear equations of motion for a rigid aircraft in the body-fixed frame are given by Wang (2019):

$$\begin{bmatrix}\dot{\boldsymbol{V}}\\ \dot{\boldsymbol{\omega}}\end{bmatrix}=\begin{bmatrix}m\boldsymbol{I} & \boldsymbol{0}\\ \boldsymbol{0} & \boldsymbol{J}\end{bmatrix}^{-1}\begin{bmatrix}-m\tilde{\boldsymbol{\omega}}\boldsymbol{V}+\boldsymbol{F}\\ -m\tilde{\boldsymbol{\omega}}\boldsymbol{J}\boldsymbol{\omega}+\boldsymbol{M}\end{bmatrix} \tag{1}$$

where $\boldsymbol{V}=[u,v,w]^{\mathsf{T}}$ and $\boldsymbol{\omega}=[p,q,r]^{\mathsf{T}}$ represent the translation and rotational velocities of the body-fixed frame relative to the inertial frame. m is the total mass. $\boldsymbol{J}$ represents the inertia matrix, which is defined as

$$\boldsymbol{J}=\begin{bmatrix}I_{xx} & 0 & -I_{xz}\\ 0 & I_{yy} & 0\\ -I_{xz} & 0 & I_{zz}\end{bmatrix} \tag{2}$$

where $I_{xx}, I_{yy}, I_{zz}, I_{xz}$ are second moments of inertia. The $\tilde{(\cdot)}$ denotes the skew symmetric matrix of the corresponding vector. $\boldsymbol{F}$ and $\boldsymbol{M}$ are the total force and moment vectors, which incorporate gravitational, aerodynamic, and thrust forces and moments. A typical aerodynamic model for a fixed-wing aircraft is give in the form of:

$$\begin{aligned}\boldsymbol{M}_a=&\bar{q}S\mathrm{diag}([b,\bar{c},b])\left(\begin{bmatrix}C_l(\beta,r,p,Ma)\\ C_m(\alpha,q,Ma)\\ C_n(\beta,r,p,Ma)\end{bmatrix}\right.\\&\left.+\begin{bmatrix}C_l^{\delta_a}(\alpha,\beta,Ma) & 0 & C_l^{\delta_r}(\alpha,\beta,Ma)\\ 0 & C_m^{\delta_e}(\alpha,Ma) & 0\\ C_n^{\delta_a}(\alpha,\beta,Ma) & 0 & C_n^{\delta_r}(\alpha,\beta,Ma)\end{bmatrix}\begin{bmatrix}\delta_a\\ \delta_e\\ \delta_r\end{bmatrix}\right)\\ \boldsymbol{F}_a=&\bar{q}S\begin{bmatrix}C_x(\alpha,\beta,q,\delta_e,Ma)\\ C_y(\alpha,\beta,q,\delta_e,Ma)\\ C_z(\alpha,\beta,q,\delta_e,Ma)\end{bmatrix}\end{aligned} \tag{3}$$

where α and β represents the angle of attack and the sideslip angle, respectively. Ma is the Mach number. V is the airspeed, $\delta_a, \delta_e, \delta_r$ are deflections of the ailerons, elevator and rudder, respectively. C_l, C_m, C_n are the rolling, pitching, and yawing moment coefficients, respectively. The dynamic pressure is given by $\bar{q}=\frac{1}{2}\rho_a V^2$ (ρ_a is the air density). $S, b, \bar{c}$ are the wing area, wing span, and mean aerodynamic chord, respectively.

The kinematics of the sideslip angle β is derived as:

$$\begin{aligned}\dot{\beta}=&\frac{1}{\sqrt{u^2+w^2}}(F_{\beta,x}+F_{\beta,y}F_{\beta,y}+F_{\beta,z}F_{\beta,z})\\&+\frac{wp}{\sqrt{u^2+w^2}}-\frac{ur}{\sqrt{u^2+w^2}}\end{aligned} \tag{4}$$

where

$$\begin{aligned}F_{\beta,x}&=-\frac{uv}{V^2}(A_x-g\sin\theta)\\ F_{\beta,y}&=1-\frac{v^2}{V^2}(A_y-g\sin\phi\cos\theta)\\ F_{\beta,z}&=-\frac{vw}{V^2}(A_z+g\cos\phi\cos\theta)\end{aligned} \tag{5}$$

and $A=[A_x,A_y,A_z]^{\mathsf{T}}$ denotes the specific force vector, g is the gravitational acceleration.

The kinematics for Euler angles $[\phi,\theta,\psi]^{\mathsf{T}}$ are given by

$$\begin{bmatrix}\dot{\phi}\\ \dot{\theta}\\ \dot{\psi}\end{bmatrix}=\begin{bmatrix}1 & \sin\phi\tan\theta & -\cos\phi\tan\theta\\ 0 & \cos\phi & -\sin\phi\\ 0 & \sin\phi\sec\theta & \cos\phi\sec\theta\end{bmatrix}\begin{bmatrix}p\\ q\\ r\end{bmatrix} \tag{6}$$

Actuator Fault The typical aircraft actuator faults include the loss of control surface area and control surface jamming. When an aircraft is subjected to the loss of control surface area fault, the corresponding aerodynamic effects can be modeled by

$$C_i^{j'}=\mu_i C_i^j, \mu_i\in[0,1], i=l,m,n, j=\delta_a,\delta_e,\delta_r \tag{7}$$

where $(\cdot')$ indicating the post-failure condition.

If one of the ailerons is jammed at $\bar{\delta}_a$, the induced force and moment coefficients can be given by (Wang et al. (2019b))

$$\begin{aligned}&\Delta C_l=\frac{1}{2}C_l^{\delta_a}\bar{\delta}_a,\quad \Delta C_n=-\frac{1}{2}C_n^{\delta_a}\bar{\delta}_a,\quad \Delta C_y=\frac{1}{2}C_y^{\delta_a}\bar{\delta}_a,\\&\Delta C_z=\frac{C_l^{\delta_a}b}{r_{a_y}},\quad \Delta C_m=-\frac{\Delta C_l b r_{a_x}}{\bar{c}r_{a_y}}\end{aligned} \tag{8}$$

where $\boldsymbol{r}_a=[r_{a_x},r_{a_y},r_{a_z}]^{\mathsf{T}}$ is the position vector from the center of mass (c.m.) to the aerodynamic center of the jammed aileron. The induced force and moment coefficients of one-side elevator jamming at $\bar{\delta}_e$ is calculated by

$$\Delta C_z=-\frac{C_m^{\delta_e}\bar{\delta}_e\bar{c}}{2r_{e_x}},\quad \Delta C_m=\frac{1}{2}C_m^{\delta_e}\bar{\delta}_e,\quad \Delta C_l=\frac{\Delta C_z r_{e_y}}{b} \tag{9}$$

with $\boldsymbol{r}_e=[r_{ex},r_{ey},r_{ez}]^{\mathsf{T}}$ indicates the position vector from c.m. to the aerodynamic center of the jammed elevator.

Structural Damage Structural damages may lead to: the changes of aerodynamic properties, inertia properties, and control effectiveness (Nabi et al. (2018); Zhang et al. (2018)). Denote the distance vector from the original c.m. O to the new c.m. location O' as $\boldsymbol{r}_{OO'}=[r_{\Delta x},r_{\Delta y},r_{\Delta z}]^{\mathsf{T}}$. The equations of motion using the non-CM approach is given by

$$\begin{bmatrix}\dot{\boldsymbol{V}}\\ \dot{\boldsymbol{\omega}}\end{bmatrix}=\begin{bmatrix}m'\boldsymbol{I} & \tilde{\boldsymbol{S}}^{\mathsf{T}}\\ \tilde{\boldsymbol{S}} & \boldsymbol{J}'\end{bmatrix}^{-1}\begin{bmatrix}-m'\tilde{\boldsymbol{\omega}}\boldsymbol{V}-\tilde{\boldsymbol{\omega}}\tilde{\boldsymbol{S}}^{\mathsf{T}}\boldsymbol{\omega}+\boldsymbol{F}'\\ -\tilde{\boldsymbol{V}}\tilde{\boldsymbol{S}}^{\mathsf{T}}\boldsymbol{\omega}-\tilde{\boldsymbol{\omega}}\tilde{\boldsymbol{S}}\boldsymbol{V}-\tilde{\boldsymbol{\omega}}\boldsymbol{J}'\boldsymbol{\omega}+\boldsymbol{M}'\end{bmatrix} \tag{10}$$

where $\tilde{(\cdot)}$ denotes the corresponding skew-symmetric matrix of the vector $(\cdot)$. $\boldsymbol{S}=[m'r_{\Delta x},m'r_{\Delta y},m'r_{\Delta z}]^{\mathsf{T}}$ is nonzero when using the non-CM approach, which leads to coupled translational and rotational motions.

In the presence of aircraft structural damage, the aerodynamic characteristics also change (Zhang et al. (2018); Nabi et al. (2018)). The influences of wing, horizontal stabilizer and vertical tail damages on aerodynamic coefficients are summarized in Table. 2. The vertical tail loss

Table 1. The main influences of structural damages on aerodynamic coefficients.

Damaged component	Changed coefficients	New coefficients
Horizontal stabilizer	C_{m_α}, C_{m_q}	ΔC_{l_q}
Vertical tail	C_{n_β}, C_{n_r}	-
Wing	$C_{l_\alpha}, C_{l_\beta}, C_{l_p}$	$\Delta C_{l_q}, \Delta C_l(\alpha)$

will also cause reductions in static and dynamic stability on the directional axis with an approximately linear relationship with the damage scale. The aerodynamic parameter changes due to the vertical tail tip loss are listed in Eq. (11).

$$\begin{aligned} &m' = m(1-\Delta_m), \quad c'_{\text{tip}} = C_{\text{tip}}(1+\delta_{c_{\text{tip}}}),\\ &x'_{c,g} = x_{c,g}(1-\Delta_{x_{c,g}}), z'_{c,g} = z_{c,g}(1+\Delta_{z_{c,g}})\\ &I'_{xx} = I_{xx}(1-\Delta_{I_x}), \quad I'_{yy} = I_{yy}(1-\Delta_{I_y}),\\ &I'_{zz} = I_{zz}(1-\Delta_{I_z}), \quad I'_{zx} = I_{xz}(1+\Delta_{I_{xz}}) \end{aligned} \tag{11}$$

The upper bounds of the changes are $\Delta_m < 0.037$, $\delta_{c_{\text{tip}}} < 0.96$, $\Delta_{I_x} < 0.0289$, $\Delta_{I_y} < 0.021$, $\Delta_{I_y} < 0.105$, $\Delta_{I_{zx}} < 0.709$, $\Delta_{x_{c,g}} < 0.037$, $\Delta_{z_{c,g}} < 0.038$ (see Zhang et al. (2018)).

Aircraft Dynamic Model for Attitude Control The typical flight attitude control is designed to make an aircraft robustly track references in roll and pitch angles while minimizing the sideslip anlge β. The control variables for high-performance aircraft in this subsection are chosen as $\boldsymbol{y} = [\phi, \theta, \beta]^\mathsf{T}$. In a general case, the aircraft is designed to be symmetry with respect to the Oxy-plane. Thus, $I_{yz} = I_{xz} = 0$. Then the nonlinear model corresponds to the motion of a rigid-body aircraft leads to states $\boldsymbol{x}_1 = [\phi, \theta, \beta]^\mathsf{T}$, $\boldsymbol{x}_2 = [p, q, r]^\mathsf{T}$ and control input $\boldsymbol{u} = [\delta_a, \delta_e, \delta_r]^\mathsf{T}$ with the following representation:

$$\begin{cases} \dot{\boldsymbol{x}}_1 = \underbrace{\begin{bmatrix} 1 & \sin\phi\tan\theta & -\cos\phi\tan\theta \\ 0 & \cos\phi & -\sin\phi \\ \frac{w}{\sqrt{u^2+w^2}} & 0 & -\frac{u}{\sqrt{u^2+w^2}} \end{bmatrix}}_{\boldsymbol{g}_1(\boldsymbol{x}_1)} \boldsymbol{x}_2 + \underbrace{\begin{bmatrix} 0 \\ 0 \\ f_1(\boldsymbol{x}) \end{bmatrix}}_{\boldsymbol{f}_1(\boldsymbol{x})} \\ \dot{\boldsymbol{x}}_2 = \underbrace{-\boldsymbol{J}^{-1}\tilde{\boldsymbol{\omega}}\boldsymbol{J}\boldsymbol{\omega} + \boldsymbol{J}^{-1}\boldsymbol{M}_f}_{\boldsymbol{f}_2(\boldsymbol{x})} + \underbrace{\boldsymbol{J}^{-1}\boldsymbol{C}_M}_{\boldsymbol{g}_2(\boldsymbol{x})}\boldsymbol{u} \\ \boldsymbol{y} = \boldsymbol{x}_1 \end{cases} \tag{12}$$

where

$$\begin{aligned} f_1(\boldsymbol{x}_1) &= \frac{uvg\sin\theta - (V^2-v^2)g\sin\phi\cos\theta - vwg\cos\phi\cos\theta}{V^2\sqrt{u^2+w^2}} \\ &+ \frac{-uvA_x + (V^2-v^2)A_y - vwA_z}{\sqrt{u^2+w^2}} \\ \boldsymbol{C}_M &= \bar{q}S\begin{bmatrix} bC_l^{\delta_a}(\alpha,\beta,Ma) & 0 & bC_l^{\delta_r}(\alpha,\beta,Ma) \\ 0 & \bar{c}C_m^{\delta_e}(\alpha,Ma) & 0 \\ bC_n^{\delta_a}(\alpha,\beta,Ma) & 0 & bC_n^{\delta_r}(\alpha,\beta,Ma) \end{bmatrix} \\ \boldsymbol{M}_f &= \bar{q}S\begin{bmatrix} bC_l(\beta,r,p,Ma) \\ \bar{c}C_m(\alpha,q,Ma) \\ bC_n(\beta,r,p,Ma) \end{bmatrix} \end{aligned}$$

An aircraft perturbed by model uncertainties, external disturbances, structural damages, and actuator faults can be modeled as:

$$\begin{cases} \dot{\boldsymbol{x}}_1 = \boldsymbol{f}_1(\boldsymbol{x}) + \boldsymbol{g}_1(\boldsymbol{x}_1)\boldsymbol{x}_2 \\ \dot{\boldsymbol{x}}_2 = \boldsymbol{f}'_2(\boldsymbol{x}) + \boldsymbol{g}'_2(\boldsymbol{x})\boldsymbol{u} + \boldsymbol{d} \end{cases} \tag{13}$$

where $\boldsymbol{d}$ is the external disturbances caused by unknown dynamics and wind gust. $\boldsymbol{f}'_2(\boldsymbol{x})$ and $\boldsymbol{g}'_2(\boldsymbol{x})$ represent dynamics function subjected to faults/damage:

$$\begin{aligned} \boldsymbol{f}'_2(\boldsymbol{x}) =& (\frac{1}{m'}\tilde{\boldsymbol{S}}\tilde{\boldsymbol{S}} + \boldsymbol{J}')^{-1}(\tilde{\boldsymbol{S}}\tilde{\boldsymbol{\omega}}\boldsymbol{V} - \frac{1}{m'}\tilde{\boldsymbol{S}}\tilde{\boldsymbol{\omega}}\tilde{\boldsymbol{S}}\boldsymbol{\omega} \\ &- \tilde{\boldsymbol{V}}\tilde{\boldsymbol{S}}^\mathsf{T}\boldsymbol{\omega} - \tilde{\boldsymbol{\omega}}\tilde{\boldsymbol{S}}\boldsymbol{V} - \tilde{\boldsymbol{\omega}}\boldsymbol{J}'\boldsymbol{\omega} - \frac{1}{m'}\tilde{\boldsymbol{S}}\boldsymbol{F}' + \boldsymbol{M}'_f) \\ \boldsymbol{g}'_2(\boldsymbol{x}) =& \boldsymbol{J}^{-1}\boldsymbol{C}_M\boldsymbol{\Lambda} + \underbrace{\left((\frac{1}{m'}\tilde{\boldsymbol{S}}\tilde{\boldsymbol{S}} + \boldsymbol{J}')^{-1} - \boldsymbol{J}^{-1}\right)\boldsymbol{C}_M\boldsymbol{\Lambda}}_{\Delta\boldsymbol{g}_2(\boldsymbol{x})} \end{aligned} \tag{14}$$

where time varying diagonal matrix $\boldsymbol{\Lambda} = \text{diag}\{w_1, w_2, w_3\} \in \mathbb{R}^{3\times3}$ models the scaling of the control effectiveness coefficients.

The object is to design a fault-tolerant flight controller to make the output $\boldsymbol{y}$ asymptotically tracks its reference signal $\boldsymbol{y}_r = [y_{r_1}, y_{r_2}, y_{r_3}]^\mathsf{T}$ in the presence of sensing errors, model uncertainties, actuator faults, and structural damage.

3. PREDICTOR-BASED ADAPTIVE INDI CONTROL DESIGN

3.1 Conventional INDI with Fixed Gains

In Eq. (13), $V, \alpha, \beta, A_x, A_y, A_z$ are measurable. Using feedback linearization, the input-output mapping of the aircraft attitude system can be represented as

$$\begin{aligned} \ddot{\boldsymbol{y}} =& \frac{\partial[\boldsymbol{f}_1(\boldsymbol{x}_1) + \boldsymbol{g}_1(\boldsymbol{x}_1)\boldsymbol{x}_2]}{\partial\boldsymbol{x}_1}(\boldsymbol{f}_1(\boldsymbol{x}_1) + \boldsymbol{g}_1(\boldsymbol{x}_1)\boldsymbol{x}_2) + \\ & \boldsymbol{g}_1(\boldsymbol{x}_1)(\boldsymbol{f}'_2(\boldsymbol{x}) + \boldsymbol{g}'_2(\boldsymbol{x})\boldsymbol{u}) \end{aligned} \tag{15}$$

Denote

$$\begin{aligned} \boldsymbol{\alpha}(\boldsymbol{x}) =& \frac{\partial[\boldsymbol{f}_1(\boldsymbol{x}_1) + \boldsymbol{g}_1(\boldsymbol{x}_1)\boldsymbol{x}_2]}{\partial\boldsymbol{x}_1}(\boldsymbol{f}_1(\boldsymbol{x}_1) + \boldsymbol{g}_1(\boldsymbol{x}_1)\boldsymbol{x}_2) \\ &+ \boldsymbol{g}_1(\boldsymbol{x}_1)\boldsymbol{f}'_2(\boldsymbol{x}), \\ \boldsymbol{\mathcal{B}}(\boldsymbol{x}) =& \boldsymbol{g}_1(\boldsymbol{x}_1)\boldsymbol{g}'_2(\boldsymbol{x}) \end{aligned} \tag{16}$$

which further leads to

$$\ddot{\boldsymbol{y}} = \boldsymbol{\alpha}(\boldsymbol{x}) + \boldsymbol{\mathcal{B}}(\boldsymbol{x})\boldsymbol{u} \tag{17}$$

Define state $\boldsymbol{\xi} = [\phi, \dot{\phi}, \theta, \dot{\theta}, \beta, \dot{\beta}]^\mathsf{T}$. the attitude dynamics in Eq. (13) can be transformed into a canonical form as

$$\begin{aligned} \dot{\boldsymbol{\xi}} &= \boldsymbol{A}_c\boldsymbol{\xi} + \boldsymbol{B}_c[\boldsymbol{\alpha}(\boldsymbol{x}) + \boldsymbol{\mathcal{B}}(\boldsymbol{x})\boldsymbol{u}] \\ \boldsymbol{y} &= \boldsymbol{C}_c\boldsymbol{\xi} \end{aligned} \tag{18}$$

Taking the first-order Taylor series expansion of (17) around the point at $t-h$ (denoted by the subscript 0) where h is the sampling period and $\boldsymbol{x}_0 = \boldsymbol{x}(t-h), \boldsymbol{u}_0 = \boldsymbol{u}(t-h)$, we obtain the incremental dynamics

$$\begin{aligned} \ddot{\boldsymbol{y}} =& \ddot{\boldsymbol{y}}\Big|_0 + \frac{\partial[\boldsymbol{\alpha}(\boldsymbol{x}) + \boldsymbol{\mathcal{B}}(\boldsymbol{x})\boldsymbol{u}]}{\partial\boldsymbol{x}}\Big|_0\Delta\boldsymbol{x} \\ &+ \boldsymbol{\mathcal{B}}(\boldsymbol{x})\Big|_0\Delta\boldsymbol{u} + \boldsymbol{R}_1(\boldsymbol{x},\boldsymbol{u},h) \\ \triangleq& \ddot{\boldsymbol{y}}_0 + \mathcal{A}_0(\boldsymbol{x})\Delta\boldsymbol{x} + \boldsymbol{\mathcal{B}}_0(\boldsymbol{x})\Delta\boldsymbol{u} + \boldsymbol{R}_1(\boldsymbol{x},\boldsymbol{u},h) \end{aligned} \tag{19}$$

and

$$\begin{aligned} \boldsymbol{R}_1(\boldsymbol{x},\boldsymbol{u},h) =& \frac{1}{2!}\frac{\partial^2[\boldsymbol{\alpha}(\boldsymbol{x}) + \boldsymbol{\mathcal{B}}(\boldsymbol{x})\boldsymbol{u}]}{\partial^2\boldsymbol{x}}\Big|_m\Delta\boldsymbol{x}^2 \\ &+ \frac{1}{2!}\frac{\partial^2[\boldsymbol{\alpha}(\boldsymbol{x}) + \boldsymbol{\mathcal{B}}(\boldsymbol{x})\boldsymbol{u}]}{\partial\boldsymbol{x}\partial\boldsymbol{u}}\Big|_m\Delta\boldsymbol{x}\Delta\boldsymbol{u} \end{aligned} \tag{20}$$

where $(\cdot)|_m$ means the evaluating $(\cdot)$ at the neighborhood where $\boldsymbol{x}_m \in [\boldsymbol{x}(t-h), \boldsymbol{x}]$ and $\boldsymbol{u}_m \in [\boldsymbol{u}(t-h), \boldsymbol{u}]$; $\Delta\boldsymbol{x}$ and $\Delta\boldsymbol{u}$ represent the state and control increments.

Denote $\boldsymbol{r} = [y_{r_1}, \dot{y}_{r_1}, y_{r_2}, \dot{y}_{r_2}, y_{r_3}, \dot{y}_{r_3}]^\mathsf{T}$. Define the tracking error vector as $\boldsymbol{e} = \boldsymbol{\xi} - \boldsymbol{r}$. Then, the error dynamics are given by

$$\begin{aligned}\dot{\boldsymbol{e}} =&\boldsymbol{A}_c\boldsymbol{e} + \boldsymbol{B}_c(\ddot{\boldsymbol{y}}_0 + \boldsymbol{\mathcal{B}}_0(\boldsymbol{x})\Delta\boldsymbol{u} - \ddot{\boldsymbol{y}}_r \\ &+ \mathcal{A}_0(\boldsymbol{x})\Delta\boldsymbol{x} + \boldsymbol{R}_1(\boldsymbol{x},\boldsymbol{u},h))\end{aligned} \tag{21}$$

The incremental control law for stabilizing the error dynamics is then designed as

$$\Delta\boldsymbol{u}_{\text{indi}} = \hat{\boldsymbol{\mathcal{B}}}_0^{-1}(\boldsymbol{x})\left(\boldsymbol{v}_c - \hat{\ddot{\boldsymbol{y}}}_0\right), \quad \boldsymbol{u} = \boldsymbol{u}_0 + \Delta\boldsymbol{u}_{\text{indi}} \tag{22}$$

where $\boldsymbol{v}_c = -\boldsymbol{K}\boldsymbol{e} + \ddot{\boldsymbol{y}}_r$, $\hat{\boldsymbol{\mathcal{B}}}_0(x)$ is the identified nominal model; $\hat{\ddot{\boldsymbol{y}}}_0$ is the measured or estimated signal of $\ddot{\boldsymbol{y}}_0$; $\boldsymbol{K}$ is designed to make $(\boldsymbol{A}_c - \boldsymbol{B}_c\boldsymbol{K})$ Hurwtiz. Substituting Eq. (22) into Eq. (21), we have

$$\begin{aligned}\dot{\boldsymbol{e}} =&(\boldsymbol{A}_c - \boldsymbol{B}_c\boldsymbol{K})\boldsymbol{e}+ \\ &\boldsymbol{B}_c((\boldsymbol{\mathcal{B}}_0(\boldsymbol{x})\hat{\boldsymbol{\mathcal{B}}}_0^{-1}(\boldsymbol{x}) - \boldsymbol{I})(\boldsymbol{v}_c - \hat{\ddot{\boldsymbol{y}}}_0) + \tilde{\ddot{\boldsymbol{y}}}_0 + \boldsymbol{\delta}(\boldsymbol{x},h)) \\ =&(\boldsymbol{A}_c - \boldsymbol{B}_c\boldsymbol{K})\boldsymbol{e} + \boldsymbol{B}_c\boldsymbol{\varepsilon}_{\text{indi}}\end{aligned} \tag{23}$$

with

$$\boldsymbol{\delta}(\boldsymbol{x},h) = [\mathcal{A}_0(\boldsymbol{x})\Delta\boldsymbol{x} + \boldsymbol{R}_1(\boldsymbol{x},\boldsymbol{u})]\Big|_{\boldsymbol{x}=\boldsymbol{x}_0,\boldsymbol{u}=\boldsymbol{u}_0+\Delta\boldsymbol{u}_{\text{indi}}} \tag{24}$$

$$\boldsymbol{\varepsilon}_{\text{indi}} = (\boldsymbol{\mathcal{B}}_0(\boldsymbol{x})\hat{\boldsymbol{\mathcal{B}}}_0^{-1}(\boldsymbol{x}) - \boldsymbol{I})(\boldsymbol{v}_c - \hat{\ddot{\boldsymbol{y}}}_0) + \tilde{\ddot{\boldsymbol{y}}}_0 + \boldsymbol{\delta}(\boldsymbol{x},h) \tag{25}$$

$$\tilde{\ddot{\boldsymbol{y}}}_0 = \ddot{\boldsymbol{y}}_0 - \hat{\ddot{\boldsymbol{y}}}_0 \tag{26}$$

Define the derivative error in the condition point as $\ddot{\boldsymbol{e}}_{y,0} = \ddot{\boldsymbol{y}}_0 - \ddot{\boldsymbol{y}}_{r,0}$ and the incremental reference derivative around the condition point as $\Delta\ddot{\boldsymbol{y}}_r = \ddot{\boldsymbol{y}}_r - \ddot{\boldsymbol{y}}_{r,0}$, the error dynamics can also be written as

$$\begin{aligned}\dot{\boldsymbol{e}} =&(\boldsymbol{A}_c - \boldsymbol{B}_c\boldsymbol{\mathcal{B}}_0(\boldsymbol{x})\hat{\boldsymbol{\mathcal{B}}}_0^{-1}(\boldsymbol{x})\boldsymbol{K})\boldsymbol{e} + \boldsymbol{B}_c(\ddot{\boldsymbol{y}}_0 - \ddot{\boldsymbol{y}}_r) \\ &+ \boldsymbol{B}_c(\boldsymbol{\mathcal{B}}_0(\boldsymbol{x})\hat{\boldsymbol{\mathcal{B}}}_0^{-1}(\boldsymbol{x})(\ddot{\boldsymbol{y}}_r - \hat{\ddot{\boldsymbol{y}}}_0 + \boldsymbol{\delta}(\boldsymbol{x},h)) \\ =&\underbrace{\left(\boldsymbol{A}_c - \boldsymbol{B}_c\boldsymbol{\mathcal{B}}_0(\boldsymbol{x})\hat{\boldsymbol{\mathcal{B}}}_0^{-1}(\boldsymbol{x})\boldsymbol{K}\right)}_{\boldsymbol{A}^\star(\boldsymbol{x})}\boldsymbol{e} \\ &+ \boldsymbol{B}_c\underbrace{\left(\boldsymbol{I} - \boldsymbol{\mathcal{B}}_0(\boldsymbol{x})\hat{\boldsymbol{\mathcal{B}}}_0^{-1}(\boldsymbol{x})\right)}_{\boldsymbol{\Phi}_0(\boldsymbol{x})}(\ddot{\boldsymbol{e}}_{y,0} - \Delta\ddot{\boldsymbol{y}}_r) \\ &+ \boldsymbol{B}_c\underbrace{\left[\boldsymbol{\mathcal{B}}_0(\boldsymbol{x})\hat{\boldsymbol{\mathcal{B}}}_0^{-1}(\boldsymbol{x})\tilde{\ddot{\boldsymbol{y}}}_0 + \boldsymbol{\delta}(\boldsymbol{x},h)\right]}_{\tilde{\boldsymbol{\Delta}}(\boldsymbol{z},h)} \\ =&\boldsymbol{A}^\star(\boldsymbol{x})\boldsymbol{e} + \boldsymbol{B}_c\boldsymbol{\Phi}_0(\boldsymbol{x})\ddot{\boldsymbol{e}}_{y,0} - \boldsymbol{B}_c\boldsymbol{\Phi}_0(\boldsymbol{x})\Delta\ddot{\boldsymbol{y}}_r + \boldsymbol{B}_c\tilde{\boldsymbol{\Delta}}(\boldsymbol{x},h) \\ =&\boldsymbol{A}^\star(\boldsymbol{x})\boldsymbol{e} + \boldsymbol{B}_c\boldsymbol{\Phi}_0(\boldsymbol{x})(\boldsymbol{B}_c^\mathsf{T}\dot{\boldsymbol{e}}(t-h) - \Delta\ddot{\boldsymbol{y}}_r) + \boldsymbol{B}_c\tilde{\boldsymbol{\Delta}}(\boldsymbol{x},h)\end{aligned} \tag{27}$$

Assume that the partial derivatives of $\boldsymbol{\alpha}(\boldsymbol{x})$ and $\boldsymbol{\mathcal{B}}(\boldsymbol{x})$ with respect to $\boldsymbol{x}$ of any order are bounded. Because of the continuity of $\boldsymbol{x}$, $\lim_{h\to 0}\|\Delta\boldsymbol{x}\| \to 0$. Therefore, $\lim_{h\to 0}\|\boldsymbol{\delta}(\boldsymbol{x},h)\| \to 0$. This inquality indicates that $\forall\bar{\delta} > 0$, $\exists\bar{h} > 0$, such that $\|\boldsymbol{\delta}(\boldsymbol{x},h)\| \le \bar{\delta}$, for all $h \in (0,\bar{h})$. In other words, there exists a h that guarantees the boundedness of $\boldsymbol{\delta}(\boldsymbol{x},h)$. Since $\tilde{\ddot{\boldsymbol{y}}}_0$, $\boldsymbol{y}_r \in \mathcal{L}_\infty$ and $\boldsymbol{r}$ is a continuous signal by assumption, it can be shown that $\Delta\ddot{\boldsymbol{y}}_r, \tilde{\Delta}(\boldsymbol{z},h) \in \mathcal{L}_\infty$.

Using the Laplace transform, we obtain the polynomial equation for the system (27)

$$\boldsymbol{D}(s) = s(\boldsymbol{I} - \boldsymbol{B}_c\boldsymbol{\Phi}_0(\boldsymbol{x})\boldsymbol{B}_c^\mathsf{T}e^{-hs}) - \boldsymbol{A}^\star(\boldsymbol{x}) \tag{28}$$

Define $\lambda_0 = \sup\{\text{Re}(s)|\det(\boldsymbol{D}(s)) = 0\}$. The system (27) is stable only if $\lambda_0 < 0$. Thus, it is common for current INDI method design to assume that the model uncertainties will satisfying the condition $\|\boldsymbol{\Phi}_0(\boldsymbol{x})\| \le \bar{b} < 1$ and the sampling period h is small enough, which could ensure $\lambda_0 < 0$. However, in harsh scenarios, $\|\boldsymbol{\Phi}_0(\boldsymbol{x})\| > 1$ can happen. The multiplicative uncertainties in the matrix $\boldsymbol{\mathcal{B}}_0(\boldsymbol{x})$ and delay in the measurement of angular accelerations could violate the stability condition of INDI control.

3.2 Predictor-Based INDI Design

In this paper, we focus on improving robustness against control effectiveness matrix uncertainties caused by model uncertainties, structural damages, and actuator faults. The condition $\|\boldsymbol{\Phi}_0(\boldsymbol{x})\| < 1$ can be violated in severe damage cases or disturbing environment. Adaptive control techniques can be used to estimate these parametric uncertainties to augment the INDI control law and to enhance robustness against uncertainties.

The incremental input-output mapping of the system can be rewritten in the form

$$\ddot{\boldsymbol{y}} = \ddot{\boldsymbol{y}}_0 + \bar{\boldsymbol{\mathcal{B}}}_0(\boldsymbol{x})\boldsymbol{\Lambda}\Delta\boldsymbol{u} + \boldsymbol{\Delta}_u(\boldsymbol{x},\boldsymbol{u},h) \tag{29}$$

where $\bar{\boldsymbol{\mathcal{B}}}_0(\boldsymbol{x}) \in \mathbb{R}^{3\times 3}$ is the known norminal control matrix, $\boldsymbol{\Lambda}$ is unknown slow time-varying control degradation matrix , $\boldsymbol{\Delta}_u(\boldsymbol{x},\boldsymbol{u},h)$ indicates the model uncertainty terms as continuous functions of $\boldsymbol{x},\boldsymbol{u},h$.

Assumption 1. The unknown nonlinear time-varying state-dependent uncertainty $\boldsymbol{\Delta}_u(\boldsymbol{x},\boldsymbol{u},h)$ can be linearly parameterized as

$$\boldsymbol{\Delta}_u(\boldsymbol{x},\boldsymbol{u},h) = \boldsymbol{W}_u^\mathsf{T}\boldsymbol{\phi}_u(\boldsymbol{x},\boldsymbol{u},h) + \boldsymbol{\varepsilon}_u \tag{30}$$

where $\boldsymbol{W}_u \in \mathbb{R}^{q_u\times 3}$ is an unknown slow time-varying parametric matrix that satisfies $\|\boldsymbol{W}_u\| \le w_u^\star$ and $\boldsymbol{\phi}_u(\boldsymbol{x}) : \mathbb{R}^9 \to \mathbb{R}^{q_u}$ is a set of known basis functions, $\boldsymbol{\varepsilon}_u$ is the bounded state-independent disturbance with $\|\boldsymbol{\varepsilon}_u\| \le \epsilon^\star$.

Assumption 2. We also assume that the control direction $\text{sign}(\boldsymbol{\Lambda})$ is known and the faulty system is controllable.

For a controllable system, given a desired Hurwitz matrix $\boldsymbol{A}_{\text{ref}}$, there must exist a possible unknown gain matrix $\boldsymbol{K}_x(\boldsymbol{x})$, such that

$$\boldsymbol{A}_{\text{ref}} = \boldsymbol{A}_c + \boldsymbol{B}_c\bar{\boldsymbol{\mathcal{B}}}_0(\boldsymbol{x})\boldsymbol{\Lambda}\boldsymbol{K}_x(\boldsymbol{x}) = \boldsymbol{A}_c - \boldsymbol{B}_c\boldsymbol{K} \tag{31}$$

Using (31) and (30), we rewrite the error system dynamics in (21) as

$$\begin{aligned}\dot{\boldsymbol{e}} =&\boldsymbol{A}_{\text{ref}}\boldsymbol{e} + \boldsymbol{B}_c\bar{\boldsymbol{\mathcal{B}}}_0(\boldsymbol{x})\boldsymbol{\Lambda}[\Delta\boldsymbol{u} - \boldsymbol{K}_x(\boldsymbol{x})\boldsymbol{e} \\ &+ \underbrace{\boldsymbol{\Lambda}^{-1}\bar{\boldsymbol{\mathcal{B}}}_0^{-1}(\boldsymbol{x})}_{\boldsymbol{K}_v(\boldsymbol{x})}(\ddot{\boldsymbol{y}}_0 + \boldsymbol{W}_u^\mathsf{T}\boldsymbol{\phi}_u(\boldsymbol{x},\boldsymbol{u}) + \boldsymbol{\varepsilon}_u - \ddot{\boldsymbol{y}}_r)]\end{aligned} \tag{32}$$

The predictor-based gain adaptive INDI control input $\Delta\boldsymbol{u}_{\text{p-indi}}$ is proposed as

$$\Delta\boldsymbol{u}_{\text{p-indi}} = \hat{\boldsymbol{K}}_x(\boldsymbol{x})\boldsymbol{e} - \hat{\boldsymbol{K}}_v(\boldsymbol{x})(\hat{\ddot{\boldsymbol{y}}}_0 + \hat{\boldsymbol{W}}_u^\mathsf{T}\boldsymbol{\phi}_u(\boldsymbol{x},\boldsymbol{u}) - \ddot{\boldsymbol{y}}_r) \tag{33}$$

where $\hat{\boldsymbol{K}}_x \in \mathbb{R}^{3\times 3}$, $\hat{\boldsymbol{K}}_v \in \mathbb{R}^{3\times 3}$ and $\hat{\boldsymbol{W}}_u \in \mathbb{R}^{q_u\times 3}$ are adaptive time-varying matrices, for which the dynamics will be defined later.

Substituting Eq. (33) into Eq. (32), yields

$$\begin{aligned}\dot{\boldsymbol{e}} =&\boldsymbol{A}_{\text{ref}}\boldsymbol{e} + \boldsymbol{B}_c\bar{\boldsymbol{\mathcal{B}}}_0(\boldsymbol{x})\boldsymbol{\Lambda}(\tilde{\boldsymbol{K}}_x(\boldsymbol{x})\boldsymbol{e} \\ &- \tilde{\boldsymbol{K}}_v(\boldsymbol{x})(\hat{\ddot{\boldsymbol{y}}}_0 + \hat{\boldsymbol{W}}_u^\mathsf{T}\boldsymbol{\phi}_u(\boldsymbol{x},\boldsymbol{u}) - \ddot{\boldsymbol{y}}_r)) \\ &+ \boldsymbol{B}_c(\tilde{\ddot{\boldsymbol{y}}}_0 + \tilde{\boldsymbol{W}}_u^\mathsf{T}\boldsymbol{\phi}_u(\boldsymbol{x},\boldsymbol{u}) + \boldsymbol{\varepsilon}_u)\end{aligned} \tag{34}$$

where $\tilde{\boldsymbol{K}}_x(\boldsymbol{x}) = \hat{\boldsymbol{K}}_x(\boldsymbol{x}) - \boldsymbol{K}_x(\boldsymbol{x})$, $\tilde{\boldsymbol{W}}_u = \hat{\boldsymbol{W}}_u - \boldsymbol{W}_u$, and $\tilde{\boldsymbol{K}}_v(\boldsymbol{x}) = \hat{\boldsymbol{K}}_v(\boldsymbol{x}) - \boldsymbol{K}_v(\boldsymbol{x})$.

The incremental predictor dynamics are formulated as

$$\dot{\boldsymbol{z}} = \boldsymbol{A}_{\text{prd}}(\boldsymbol{z}-\boldsymbol{e}) + \boldsymbol{A}_{\text{ref}}\boldsymbol{e} \tag{35}$$

Let $\hat{\boldsymbol{e}} = \boldsymbol{z}-\boldsymbol{e}$ represents the prediction errors. The tracking and prediction error dynamics can be derived as

$$\begin{aligned}\dot{\boldsymbol{e}} =& \boldsymbol{A}_{\text{ref}}\boldsymbol{e} - \boldsymbol{B}_c\bar{\boldsymbol{\mathcal{B}}}_0(\boldsymbol{x})\boldsymbol{\Lambda}\tilde{\boldsymbol{K}}_v(\boldsymbol{x})(\hat{\ddot{\boldsymbol{y}}}_0 + \hat{\boldsymbol{W}}_u^{\mathsf{T}}\boldsymbol{\phi}_u(\boldsymbol{x},\boldsymbol{u}) - \ddot{\boldsymbol{y}}_r)\\ &+\boldsymbol{B}_c\bar{\boldsymbol{\mathcal{B}}}_0(\boldsymbol{x})\boldsymbol{\Lambda}\tilde{\boldsymbol{K}}_x(\boldsymbol{x})\boldsymbol{e} + \boldsymbol{B}_c(\tilde{\ddot{\boldsymbol{y}}}_0 + \tilde{\boldsymbol{W}}_u^{\mathsf{T}}\boldsymbol{\phi}_u(\boldsymbol{x},\boldsymbol{u}) + \boldsymbol{\varepsilon}_u)\\ \dot{\hat{\boldsymbol{e}}} =& \boldsymbol{A}_{\text{prd}}\hat{\boldsymbol{e}} + \boldsymbol{B}_c\bar{\boldsymbol{\mathcal{B}}}_0(\boldsymbol{x})\boldsymbol{\Lambda}\tilde{\boldsymbol{K}}_v(\boldsymbol{x})(\hat{\ddot{\boldsymbol{y}}}_0 + \hat{\boldsymbol{W}}_u^{\mathsf{T}}\boldsymbol{\phi}_u(\boldsymbol{x},\boldsymbol{u}) - \ddot{\boldsymbol{y}}_r)\\ &-\boldsymbol{B}_c\bar{\boldsymbol{\mathcal{B}}}_0(\boldsymbol{x})\boldsymbol{\Lambda}\tilde{\boldsymbol{K}}_x(\boldsymbol{x})\boldsymbol{e} - \boldsymbol{B}_c(\tilde{\ddot{\boldsymbol{y}}}_0 + \tilde{\boldsymbol{W}}_u^{\mathsf{T}}\boldsymbol{\phi}_u(\boldsymbol{x},\boldsymbol{u}) + \boldsymbol{\varepsilon}_u)\end{aligned} \tag{36}$$

Choose the following predictor-based adaptive laws:

$$\begin{aligned}&\hat{\boldsymbol{K}}_x(\boldsymbol{x}) = -\hat{\boldsymbol{\Upsilon}}\bar{\boldsymbol{\mathcal{B}}}_0^{-1}(\boldsymbol{x})\boldsymbol{K}, \quad \hat{\boldsymbol{K}}_v(\boldsymbol{x}) = \hat{\boldsymbol{\Upsilon}}\bar{\boldsymbol{\mathcal{B}}}_0^{-1}(\boldsymbol{x})\\ &\dot{\hat{\boldsymbol{\Upsilon}}} = \boldsymbol{\Gamma}_e[\bar{\boldsymbol{\mathcal{B}}}_0^{-1}(\boldsymbol{x})(\hat{\ddot{\boldsymbol{y}}}_0 + \hat{\boldsymbol{W}}_u^{\mathsf{T}}\boldsymbol{\phi}_u(\boldsymbol{x},\boldsymbol{u}) - \dot{\boldsymbol{y}}_r)\\ &\qquad + \bar{\boldsymbol{\mathcal{B}}}_0^{-1}(\boldsymbol{x})\boldsymbol{K}\boldsymbol{e}]\bar{\boldsymbol{e}}^{\mathsf{T}}\bar{\boldsymbol{\mathcal{B}}}_0(\boldsymbol{x})\text{sign}(\boldsymbol{\Lambda})\\ &\dot{\hat{\boldsymbol{W}}} = -\boldsymbol{\Gamma}_w\boldsymbol{\phi}_u(\boldsymbol{x},\boldsymbol{u})\bar{\boldsymbol{e}}^{\mathsf{T}}\end{aligned} \tag{37}$$

where $\boldsymbol{\Gamma}_e = \boldsymbol{\Gamma}_e^{\mathsf{T}} > 0$, $\boldsymbol{\Gamma}_w = \boldsymbol{\Gamma}_w^{\mathsf{T}} > 0$, and $\bar{\boldsymbol{e}}^{\mathsf{T}} = (\boldsymbol{e}^T\boldsymbol{P}_{\text{ref}} - \hat{\boldsymbol{e}}^T\boldsymbol{P}_{\text{prd}})\boldsymbol{B}_c$.

Theorem 3. If Assumptions 1-2 are satisfied for the attitude dynamics in Eq. (29), then using the proposed predictor-based control law in Eq. (33) with the adaptive gains in Eq. (37), the aircraft attitude tracking error $\boldsymbol{e}$ and predictor error $\hat{\boldsymbol{e}}$ in Eq. (36) are globally ultimately bounded.

Proof. Consider the following candidate Lyapunov function:

$$\begin{aligned}V =& \boldsymbol{e}^{\mathsf{T}}\boldsymbol{P}_{\text{ref}}\boldsymbol{e} + \hat{\boldsymbol{e}}^{\mathsf{T}}\boldsymbol{P}_{\text{prd}}\hat{\boldsymbol{e}}\\ &+ \text{trace}(\tilde{\boldsymbol{\Upsilon}}^{\mathsf{T}}\boldsymbol{\Gamma}_e^{-1}\tilde{\boldsymbol{\Upsilon}}|\boldsymbol{\Lambda}|) + \text{trace}(\tilde{\boldsymbol{W}}^{\mathsf{T}}\boldsymbol{\Gamma}_w^{-1}\tilde{\boldsymbol{W}})\end{aligned} \tag{38}$$

where $\boldsymbol{P}_{\text{ref}} = \boldsymbol{P}_{ref}^{\mathsf{T}} > 0$, $\boldsymbol{P}_{\text{prd}} = \boldsymbol{P}_{\text{prd}}^{\mathsf{T}} > 0$, and

$$\begin{aligned}\boldsymbol{A}_{ref}^{\mathsf{T}}\boldsymbol{P}_{\text{ref}} + \boldsymbol{P}_{\text{ref}}\boldsymbol{A}_{\text{ref}} = -\boldsymbol{Q}_{\text{ref}},\\ \boldsymbol{A}_{prd}^{\mathsf{T}}\boldsymbol{P}_{\text{prd}} + \boldsymbol{P}_{\text{prd}}\boldsymbol{A}_{\text{prd}} = -\boldsymbol{Q}_{\text{prd}}\end{aligned} \tag{39}$$

with positive definite matrices $\boldsymbol{Q}_{\text{ref}}$ and $\boldsymbol{Q}_{\text{prd}}$.

For simplicity in the notation, the arguments of the time-dependent and state-dependent vectors and matrices are omitted in the rest of this paper. The time derivative of V evaluated along Eq. (36) yields

$$\begin{aligned}\dot{V} =& -\boldsymbol{e}^{\mathsf{T}}\boldsymbol{Q}_{\text{ref}}\boldsymbol{e} - \hat{\boldsymbol{e}}^{\mathsf{T}}\boldsymbol{Q}_{\text{prd}}\hat{\boldsymbol{e}}\\ &+ 2(\boldsymbol{e}^{\mathsf{T}}\boldsymbol{P}_{\text{ref}} - \hat{\boldsymbol{e}}^{\mathsf{T}}\boldsymbol{P}_{\text{prd}})\boldsymbol{B}_c\bar{\boldsymbol{\mathcal{B}}}_0\boldsymbol{\Lambda}\tilde{\boldsymbol{K}}_x\boldsymbol{e}\\ &- 2(\boldsymbol{e}^{\mathsf{T}}\boldsymbol{P}_{\text{ref}} - \hat{\boldsymbol{e}}^{\mathsf{T}}\boldsymbol{P}_{\text{prd}})\boldsymbol{B}_c\bar{\boldsymbol{\mathcal{B}}}_0\boldsymbol{\Lambda}\tilde{\boldsymbol{K}}_v(\hat{\ddot{\boldsymbol{y}}}_0 - \ddot{\boldsymbol{y}})\\ &- 2(\boldsymbol{e}^{\mathsf{T}}\boldsymbol{P}_{\text{ref}} - \hat{\boldsymbol{e}}^{\mathsf{T}}\boldsymbol{P}_{\text{prd}})\boldsymbol{B}_c\bar{\boldsymbol{\mathcal{B}}}_0\boldsymbol{\Lambda}\tilde{\boldsymbol{K}}_v\hat{\boldsymbol{W}}_u^{\mathsf{T}}\boldsymbol{\phi}_u\\ &+ 2(\boldsymbol{e}^{\mathsf{T}}\boldsymbol{P}_{\text{ref}} - \hat{\boldsymbol{e}}^{\mathsf{T}}\boldsymbol{P}_{\text{prd}})\boldsymbol{B}_c(\tilde{\ddot{\boldsymbol{y}}}_0 + \tilde{\boldsymbol{W}}_u^{\mathsf{T}}\boldsymbol{\phi}_u + \boldsymbol{\varepsilon}_u)\\ &+ 2\,\text{trace}(\tilde{\boldsymbol{\Upsilon}}^{\mathsf{T}}\boldsymbol{\Gamma}_e^{-1}\dot{\hat{\boldsymbol{\Upsilon}}}|\boldsymbol{\Lambda}|) + 2\,\text{trace}(\tilde{\boldsymbol{W}}^{\mathsf{T}}\boldsymbol{\Gamma}_e^{-1}\dot{\hat{\boldsymbol{W}}})\\ =& -\boldsymbol{e}^{\mathsf{T}}\boldsymbol{Q}_{\text{ref}}\boldsymbol{e} - \hat{\boldsymbol{e}}^{\mathsf{T}}\boldsymbol{Q}_{\text{prd}}\hat{\boldsymbol{e}} - 2\bar{\boldsymbol{e}}^{\mathsf{T}}\bar{\boldsymbol{\mathcal{B}}}_0\boldsymbol{\Lambda}\tilde{\boldsymbol{\Upsilon}}\bar{\boldsymbol{\mathcal{B}}}_0^{-1}\boldsymbol{K}\boldsymbol{e}\\ &- 2\bar{\boldsymbol{e}}^{\mathsf{T}}\bar{\boldsymbol{\mathcal{B}}}_0\boldsymbol{\Lambda}\tilde{\boldsymbol{\Upsilon}}\bar{\boldsymbol{\mathcal{B}}}_0^{-1}(\hat{\ddot{\boldsymbol{y}}}_0 + \hat{\boldsymbol{W}}_u^{\mathsf{T}}\boldsymbol{\phi}_u - \ddot{\boldsymbol{y}}_r)\\ &+ 2\bar{\boldsymbol{e}}^{\mathsf{T}}(\tilde{\ddot{\boldsymbol{y}}}_0 + \tilde{\boldsymbol{W}}_u^{\mathsf{T}}\boldsymbol{\phi}_u + \boldsymbol{\varepsilon}_u)\\ &+ 2\,\text{trace}(\tilde{\boldsymbol{\Upsilon}}^{\mathsf{T}}\boldsymbol{\Gamma}_e^{-1}\dot{\hat{\boldsymbol{\Upsilon}}}|\boldsymbol{\Lambda}|) + 2\,\text{trace}(\tilde{\boldsymbol{W}}^{\mathsf{T}}\boldsymbol{\Gamma}_w^{-1}\dot{\hat{\boldsymbol{W}}})\\ =& -\boldsymbol{e}^{\mathsf{T}}\boldsymbol{Q}_{\text{ref}}\boldsymbol{e} - \hat{\boldsymbol{e}}^{\mathsf{T}}\boldsymbol{Q}_{\text{prd}}\hat{\boldsymbol{e}} + 2\bar{\boldsymbol{e}}^{\mathsf{T}}(\tilde{\ddot{\boldsymbol{y}}}_0 + \boldsymbol{\varepsilon}_u)\\ &+ 2\,\text{trace}(\tilde{\boldsymbol{W}}^{\mathsf{T}}(\boldsymbol{\Gamma}_w^{-1}\dot{\hat{\boldsymbol{W}}} + \boldsymbol{\phi}_u\bar{\boldsymbol{e}}^{\mathsf{T}}))\\ &+ 2\,\text{trace}(\tilde{\boldsymbol{\Upsilon}}^{\mathsf{T}}(\boldsymbol{\Gamma}_w^{-1}\dot{\hat{\boldsymbol{\Upsilon}}} - \bar{\boldsymbol{\mathcal{B}}}_0^{-1}\boldsymbol{K}\boldsymbol{e}\bar{\boldsymbol{e}}^{\mathsf{T}}\bar{\boldsymbol{\mathcal{B}}}_0\text{sign}(\boldsymbol{\Lambda})\\ &- \bar{\boldsymbol{\mathcal{B}}}_0^{-1}(\hat{\ddot{\boldsymbol{y}}}_0 + \hat{\boldsymbol{W}}_u^{\mathsf{T}}\boldsymbol{\phi}_u - \ddot{\boldsymbol{y}}_r)\bar{\boldsymbol{e}}^{\mathsf{T}}\bar{\boldsymbol{\mathcal{B}}}_0\text{sign}(\boldsymbol{\Lambda}))|\boldsymbol{\Lambda}|)\end{aligned} \tag{40}$$

Substituting the adaptive law Eq.(37) into Eq. (40), implies that

$$\begin{aligned}\dot{V} =& -\boldsymbol{e}^{\mathsf{T}}\boldsymbol{Q}_{\text{ref}}\boldsymbol{e} - \hat{\boldsymbol{e}}^{\mathsf{T}}\boldsymbol{Q}_{\text{prd}}\hat{\boldsymbol{e}}\\ &+ 2(\boldsymbol{e}^{\mathsf{T}}\boldsymbol{P}_{\text{ref}} - \hat{\boldsymbol{e}}^{\mathsf{T}}\boldsymbol{P}_{\text{prd}})\boldsymbol{B}_c(\tilde{\ddot{\boldsymbol{y}}}_0 + \boldsymbol{\varepsilon}_u)\\ &\le -\lambda_{\min}(\boldsymbol{Q}_{\text{ref}})\|\boldsymbol{e}\|^2 - \lambda_{\min}(\boldsymbol{Q}_{\text{prd}})\|\hat{\boldsymbol{e}}\|^2\\ &+ 2(\bar{\delta_0} + \epsilon^\star)(\|\boldsymbol{P}_{\text{ref}}\boldsymbol{B}_c\boldsymbol{e}\|\|\boldsymbol{P}_{\text{prd}}\boldsymbol{B}_c\hat{\boldsymbol{e}}\|)\end{aligned} \tag{41}$$

where $\bar{\delta_0} \ge \|\tilde{\ddot{\boldsymbol{y}}}_0\|$, which proves uniform ultimate boundedness of $\boldsymbol{e}$, $\hat{\boldsymbol{e}}$, $\tilde{\boldsymbol{\Upsilon}}$, $\tilde{\boldsymbol{W}}$. Since the ideal values of $\boldsymbol{\Upsilon}$,$\boldsymbol{W}$ are bounded and their estimation errors $\tilde{\boldsymbol{\Upsilon}}$, $\tilde{\boldsymbol{W}}$ are bounded, then their estimated values are bounded as well.

4. NUMERICAL SIMULATIONS

In this section, the proposed adaptive INDI control law in Sec. 3 will be numerically evaluated on a public model of F-16 Nguyen (1979). Actuators are modeled with second-order linear dynamics with rate and position limits (parameters from Table 2 of Ref. Wang et al. (2019a)). This initial airspeed $V = 600$ ft/s and altitude $h = 12000$ ft. The initial attitude states for the aircraft are $\boldsymbol{x}_1 = [0,0,0]^\circ, \boldsymbol{x}_2 = [0,0,0]^\circ$/s. Parametric uncertainties are added to the mass m, the moment of inertia $\boldsymbol{J}$, wing area S, wing span b, and mean aerodynamic chord $\bar{c}$ with a maximum of five percent. The angular acceleration sensor is modeled with first-order linear system $G(s) = \frac{1}{0.0125s+1}$. In addition, the measurement noise level of angular acceleration measurements are set to 0.1 $m.s^{-2}$.

The fault cases considered in this section include the effectiveness loss of rudder, aileron, elevator, and structural damage. The influences of actuator faults and structural damage are modeled using the method in Sec. 2. To be specific, the elevator lost 50% of its effectiveness at 3 s, the aileron lost 40% of its effectiveness and the rudder has lost 60% of the effectiveness at 5 s, respectively. Meanwhile, the uncertainties in the effectiveness for rudder, aileron, elevator with $w_1 = 1.8$ at $t = 13s$, and $w_2 = 1.3, w_3 = 1.5$ at $t = 15s$, are considered. Moreover, the right aileron runs away and get jammed at $t = 3$ s with $\bar{\delta}_a = 15.05^\circ$. Also, at $t = 5$ s, the left elevator is jammed downwards at $\bar{\delta}_e = -12.5^\circ$. Apart from these actuator faults, the right wing lost 25% of its area at $t = 3$ s, the entire left horizontal tail is lost at $t = 5$ s, and a half of the vertical tail is lost at $t = 7$ s.

For the numerical simulations presented in this section, the control parameters are set as: $\Gamma_e = \text{diag}[10,10,10]$, $\Gamma_w = 0.5$, and

$$\begin{aligned}&\boldsymbol{K} = [\text{diag}\{8,8,8\}, \text{diag}\{6,6,6\}],\\ &\boldsymbol{P}_{\text{prd}} = \text{diag}\{0.5, 0.67, 0.83, 0.4, 0.5, 0.5\}\\ &\boldsymbol{P}_{\text{ref}} = \begin{bmatrix} 8.8333 & 0 & 0 & 0.1667 & 0 & 0\\ 0 & 8.8333 & 0 & 0 & 0.1667 & 0\\ 0 & 0 & 8.8333 & 0 & 0 & 0.1667\\ 0.1667 & 0 & 0 & 0.5333 & 0 & 0\\ 0 & 0.1667 & 0 & 0 & 0.5333 & 0\\ 0 & 0 & 0.1667 & 0 & 0 & 0.5333 \end{bmatrix}\end{aligned} \tag{42}$$

The simulation results are showed in Fig. 1 - Fig. 5, which clearly show that the proposed approach exhibits excellent tracking performances for the angle of attack, sideslip angle and the bank angle in spite of multiple uncertainties, actuator faults and structural damages. In this simulated

scenario, it can be seed from Fig. 4 that $\|\mathbf{\Phi}_0(x)\| > 1$ after $t = 3$ s. Even through $\|\mathbf{\Phi}_0(\boldsymbol{x})\| > 1$ happens, the tracking performance is improved with adaptive gains (comparing Fig. 1 with Fig. 2). It can be seen from the attitude tracking responses in Fig. 2 that the proposed method has decreased tracking errors compared to the conventional INDI control with fixed gains.

It can be seen from Fig. 3 that the right aileron is jammed at $t = 3$ s and left elevator is jammed at $t = 5$ s. From the deflection of control surfaces in Figs. 3, the control amplitudes of PGA-INDI are slightly sharper than conventional INDI in some local time, which leads to a faster attitude tracking performance. The adaptation of the gains $\hat{\Gamma}$ can be observed in Figs. 5. It shows that the gains swiftly adapt to the injection of faults and uncertainties.

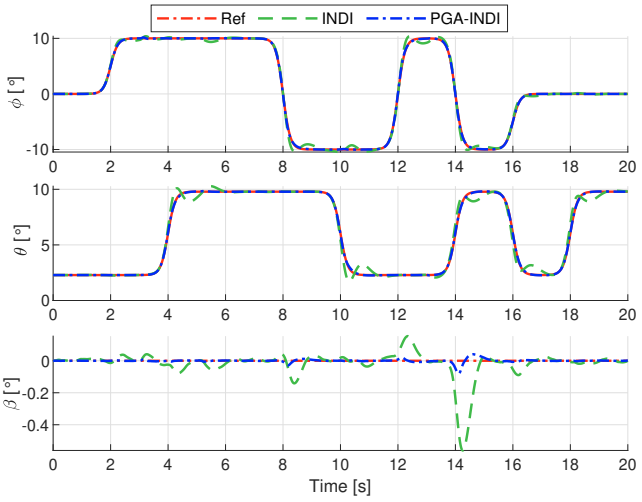

Fig. 1. Attitude tracking performance.

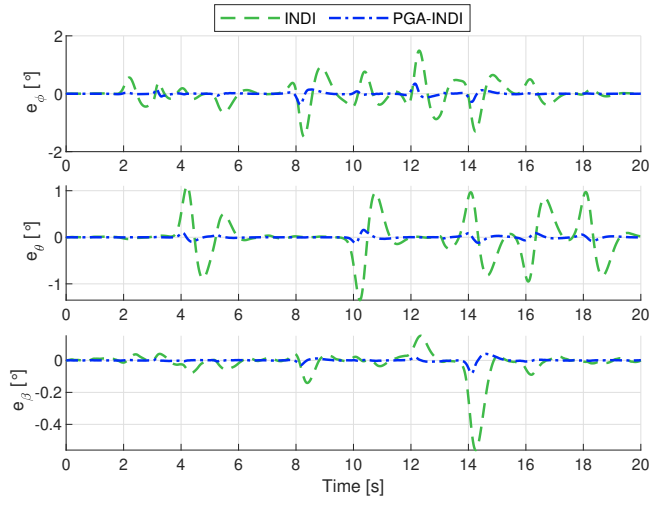

Fig. 2. Attitude tracking errors.

5. CONCLUSION

A novel adaptive INDI control method for fault accommodation of aircraft is proposed in this paper. The INDI control idea is integrated with a predictor-based adaptive law to improve the aircraft attitude tracking performance against control effectiveness uncertainties. This paper has

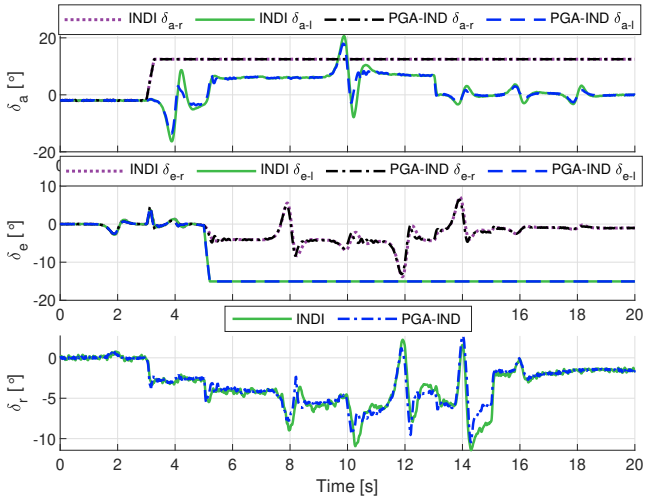

Fig. 3. Control surfaces deflection.

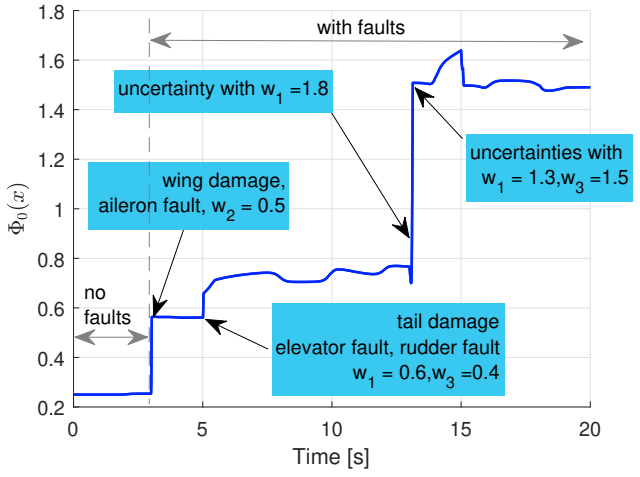

Fig. 4. The responses of $\mathbf{\Phi}_0(\boldsymbol{x})$.

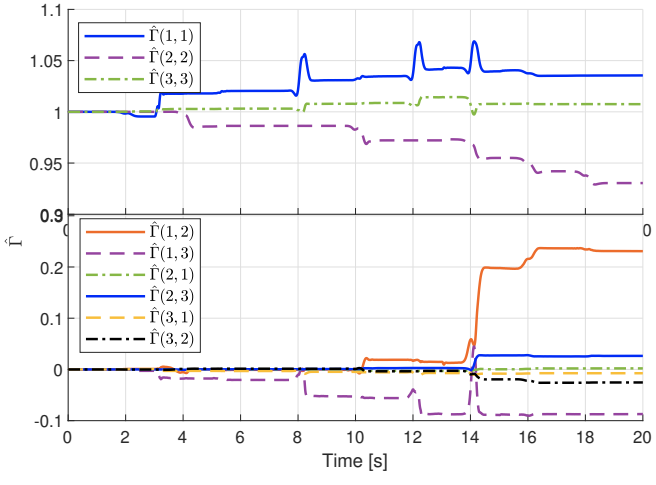

Fig. 5. The adaptive gain $\hat{\Gamma}$.

theoretically analyzed that the performance of INDI is influenced by the sensing error bound and the control effectiveness matrix estimation. Given this, this paper proposes a predictor-based adaptive incremental nonlin-

ear dynamic inverse control, denoted as PGA-INDI, with guaranteed stability. Simulations verify the effectiveness of this method on an attitude tracking problem of an aircraft subjects to sensing errors, actuator faults, and structural damage.

REFERENCES

Bošković, J.D. and Mehra, R.K. (2003). Failure detection, identification and reconfiguration in flight control. In *Fault Diagnosis and Fault Tolerance for Mechatronic Systems: Recent Advances*, 129–167. Springer.

Jeon, B.J., Seo, M.G., Shin, H.S., and Tsourdos, A. (2021). Understandings of incremental backstepping controller considering measurement delay with model uncertainty. *Aerospace Science and Technology*, 109, 106408.

Jiang, J. and Yu, X. (2012). Fault-tolerant control systems: A comparative study between active and passive approaches. *Annual Reviews in control*, 36(1), 60–72.

Keijzer, T., Looye, G., Chu, Q.P., and Van Kampen, E.J. (2019). Design and flight testing of incremental backstepping based control laws with angular accelerometer feedback. In *AIAA Scitech 2019 Forum*, 0129.

Nabi, H., Lombaerts, T., Zhang, Y., van Kampen, E., Chu, Q., and de Visser, C.C. (2018). Effects of structural failure on the safe flight envelope of aircraft. *Journal of Guidance, Control, and Dynamics*, 41(6), 1257–1275.

Nguyen, L.T. (1979). *Simulator study of stall/post-stall characteristics of a fighter airplane with relaxed longitudinal static stability*, volume 12854. National Aeronautics and Space Administration.

Sieberling, S., Chu, Q., and Mulder, J. (2010). Robust flight control using incremental nonlinear dynamic inversion and angular acceleration prediction. *Journal of guidance, control, and dynamics*, 33(6), 1732–1742.

Smeur, E.J., Chu, Q., and de Croon, G.C. (2016). Adaptive incremental nonlinear dynamic inversion for attitude control of micro air vehicles. *Journal of Guidance, Control, and Dynamics*, 39(3), 450–461.

Sun, S., Wang, X., Chu, Q., and de Visser, C. (2020). Incremental nonlinear fault-tolerant control of a quadrotor with complete loss of two opposing rotors. *IEEE Transactions on Robotics*, 37(1), 116–130.

van Ekeren, W., Looye, G., Kuchar, R.O., Chu, Q.P., and van Kampen, E.J. (2018). Design, implementation and flight-tests of incremental nonlinear flight control methods. 384. American Institute of Aeronautics and Astronautics.

Wang, X. (2019). *Incremental sliding mode flight control*. Ph.D. thesis. URL `http://resolver.tudelft.nl/uuid: c8259a08-bbee-4af0-b570-1350a2dd8d89`.

Wang, X., van Kampen, E.J., Chu, Q., and Lu, P. (2019a). Incremental sliding-mode fault-tolerant flight control. *Journal of guidance, control, and dynamics*, 42(2), 244–259.

Wang, X., Van Kampen, E.J., Chu, Q., and Lu, P. (2019b). Stability analysis for incremental nonlinear dynamic inversion control. *Journal of Guidance, Control, and Dynamics*, 42(5), 1116–1129.

Zhang, Y., De Visser, C., and Chu, Q. (2018). Aircraft damage identification and classification for database-driven online flight-envelope prediction. *Journal of Guidance, Control, and Dynamics*, 41(2), 449–460.

Zhang, Y. and Jiang, J. (2008). Bibliographical review on reconfigurable fault-tolerant control systems. *Annual reviews in control*, 32(2), 229–252.

Zolghadri, A., Henry, D., Cieslak, J., Efimov, D., and Goupil, P. (2014). *Fault diagnosis and fault-tolerant control and guidance for aerospace vehicles*, volume 236. Springer.